Hindawi
Journal of Nanomaterials
Volume 2018, Article ID 2417949, 7 pages
https://doi.org/10.1155/2018/2417949

Research Article

New In Situ Synthesis Method for Fe_3O_4/Flake Graphite Nanosheet Composite Structure and Its Application in Anode Materials of Lithium-Ion Batteries

Chenhao Qian,[1,2] Ziyang He,[3] Chen Liang,[4] and Weixi Ji[1,2]

[1]*Department of Mechanical Engineering, Jiangnan University, Wuxi, Jiangsu 214122, China*
[2]*Jiangsu Key Laboratory of Advanced Food Manufacturing Equipment and Technology, Jiangnan University, Wuxi, Jiangsu 214122, China*
[3]*Department of Computer Science, Columbia University, New York, NY 10027, USA*
[4]*School of Engineering, University of Liverpool, Brownlow Hill, Liverpool L69 3GH, UK*

Correspondence should be addressed to Ziyang He; zh2330@columbia.edu and Weixi Ji; jiweixi@jiangnan.edu.cn

Received 29 October 2017; Revised 2 February 2018; Accepted 8 February 2018; Published 15 March 2018

Academic Editor: Nam-Jung Kim

High-pressure torsion (HPT), a severe plastic deformation (SPD) method, is rarely used in the manufacturing process of functional materials. In the present work, the authors creatively proposed using HPT as an alternative method an approach for high energy ball-milling in the preparation of an Fe_3O_4 and lamellar graphite nanosheet (GNS) composite material. The corresponding electrochemical experiments verified that the in situ synthesized Fe_3O_4/GNS composite material has good lithium-storage performance and that it can retain good capacity (548.2 mA h g^{-1}) even after several hundred cycles with high current density (8 C). Meanwhile, this performance has directly confirmed that SPD technique has great potential for the preparation of anode materials of lithium-ion batteries, especially in manufacturing metallic functional nanomaterials.

1. Introduction

Future high-end communications, portable devices, and electric vehicles present great demands for lithium-ion batteries (LIBs) with high power density, high energy density, and good cycling stability. Tarascon and Armand [1] presented the development of lithium-based rechargeable batteries and demonstrated that graphite is the anode material used in commercial LIBs. Zhu et al. [2] prepared a promising route for a large-scale production of reduced graphene oxide platelet/metal oxide nanoparticle composites as electrode materials for Li-ion batteries. The rate capability of various lithium-ion half-cells was investigated by Buqa et al. [3] and the results showed that high current performance of these cells was restricted with a theoretical capacity of 372 mA h g^{-1}, which cannot satisfy the requirements for the new generation of LIBs. Thus, development of new types of electrode materials is urgent. Arico et al. [4] describes some recent developments in the discovery of nanoelectrolytes and nanoelectrodes for lithium batteries. Jang et al. [5] present a direct synthesis of ferrite/carbon hybrid nanosheets for high performance lithium-ion battery anodes. Because of their merits (high theoretical capacities and abundant resources), various transition metal oxides have been widely and intensively studied with respect to becoming anode materials for LIBs, such as α-Fe_2O_3 submicron spheres with different internal structures [6], nanorod-like Fe_2O_3/graphene nanocomposite [7], bicontinuous mesoporous nanostructure Fe_3O_4 [8], carbon-encapsulated Fe_3O_4 nanoparticles [9], MnO_2 nanoparticles [10], layered birnessite-type MnO_2 [11], Co_3O_4 nanoparticles [12], Co_3O_4 nanorods [13], mesoporous TiO_2 thin films [14], and TiO_2 nanoparticles [15]. Wu et al. [16] verified that these kinds of oxides for lithium-ion batteries (LIBs) did satisfy the ever-growing demands for better performance. Reddy et al. [17] also presented their use in a wide range of applications. Among the transition metal oxides that have been studied, Fe_3O_4 has received much attention because of its high theoretical capacity

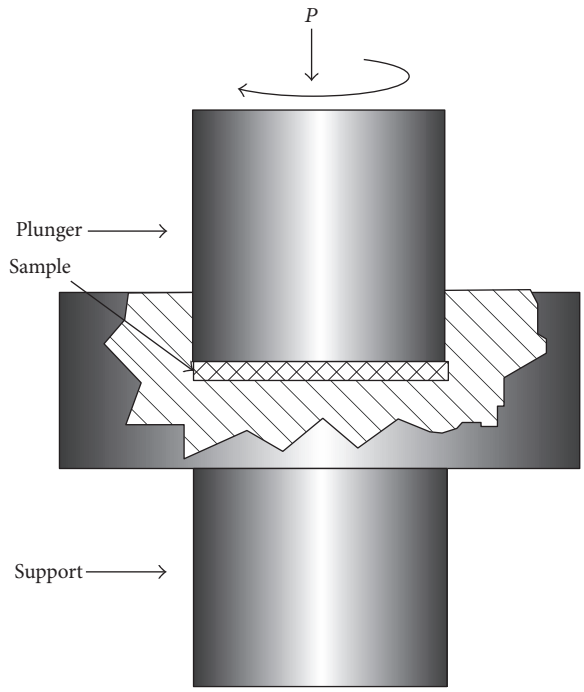

Figure 1: Schematic diagram of high-pressure torsion experiment.

(926 mA h·g^{-1}) and low cost. However, large structure and volume changes (around 180%) occur in the material after the lithium-storage reaction, because the lithium-storage mechanism of Fe_3O_4 is a chemical transition that produces elementary Fe and Li_2O particles, and the fine particles of elementary Fe are adsorbed on Li_2O surface. The substantial changes lead to structural damage and decrease the electronic conductivity, thus resulting in a shorter cycling life. In addition, the irreversible capacity in the first cycle will be large because of the irreversible formation of Li_2O (SEI layer). One of the commonly used modification approaches is combining Fe_3O_4 and other materials to relieve and inhibit the volume expansion. Carbon materials, such as amorphous carbon, graphene, and carbon nanotubes, are often used in this approach. Zhuo et al. [18] prepared an Fe_3O_4/graphene nanocomposite, and a capacity of 1026 mA h·g^{-1} was maintained after 30 charge-discharge cycles at a current density of 35 mA·g^{-1} within a voltage range of 0.0–3.0 V. Also, a high reversible capacity of 580 mA h·g^{-1} was maintained at a current density of 700 mA·g^{-1} for 100 cycles, indicating excellent cycling stability and a high-rate discharging capability. Lian et al. [19] synthesized an Fe_3O_4/graphene nanocomposite using a hydrothermal method, and the composite also exhibited excellent performance with a capacity of 1045 mA·g^{-1} maintained after 40 charge-discharge cycles at a current density of 100 mA/g and within a voltage range of 0.01–3.00 V.

Indeed, hydrothermal synthesis and surface modification following preparation can provide a valid approach for a conventional Fe_3O_4 nanostructure. However, yield and cost restrict this approach. Therefore, this approach may currently only be achieved in lab environments and is still a long way from large-scale industrial manufacturing. In comparison, severe plastic deformation (SPD) is novel technology that can be used to prepare bulk ultrafine crystalline materials via a mechanical method. The SPD method can be used in the preparation of a relatively large volume of ultrafine grain samples that have nanoscale grain size microstructure. High-pressure torsion (HPT) is an SPD method that applies torque at the cross-section along with axial compression to change the frictional resistance into frictional force. Therefore, the HPT method simultaneously achieves a certain torsional deflection and simple compressive torsion. The schematic diagram of this method can be seen in Figure 1. This method was modified by Valiev [20] to study phase changes under SPD and changes in organizational structure after SPD. They found that, after HPT, a uniform nanostructure with large-angle grain boundaries appeared and that qualitative changes greatly enhanced the corresponding mechanical properties. These findings led to the HPT method to become a new approach for synthesizing nanomaterials and is considered to be one of the promising ways to achieve industrial scale manufacturing of bulk nanomaterials. In the past, this method was commonly applied in the modification of structural materials such as aluminum alloy (Xu et al., 2008), titanium alloy (Shaman et al., 2015), and tungsten alloy [21], but its application in the preparation of functional materials has rarely been reported.

Because high energy ball-milling technology has been widely used in the synthesis of functional materials, even in the exfoliation of graphene [22], in this work, the author assumed that high-pressure torsion (HPT) technique has a similar mechanism (mechanical alloying) but with even higher energy input it may be also used in the synthesis of functional materials.

2. Experiment

2.1. Materials and Pretreatment. First, pure Fe foils (99.5%, Goodwill, Beijing) that had dimensions of 2 cm × 2 cm and a thickness of 0.05 mm were used as the raw material. Flake graphite (100 mesh, Sigma-Aldrich) was placed within the multiple layers of the Fe foils for the initial rolling pretreatment, and the mass ratio of flake graphite-to-Fe foil was 14 : 1. The obtained material was then treated with HPT. The HPT chamber was 9.8 mm long and had a cavity height of 1.6 mm. The treatment pressure was 11 GPa, the treatment cycle number was 10, and the experiment temperature was room temperature (20°C). Tungsten carbide (WC) balls-assisted high energy ball-milling was conducted as a comparison group, and the ball-milling process was carried out under Ar atmosphere. The mass ratio of the balls to powders was 10 : 1 (same composite ratio as HPT sample), and the high energy ball-milling was conducted with a Fritsch Pulverisette-5 machine at a rotation rate of 500 rpm lasting for 15 h.

2.2. Chemical Oxidation and Dispersion. Acidic solution was used to oxidize the lamellar Fe nanosheets after HPT and the high energy ball-milling treatment to obtain Fe_3O_4 nanosheets. The formulation of the oxidizing solution was 0.04 mL 25% HCl added to 0.1 M KCl to obtain a solution with a pH value of 3. After the active HPT and high energy ball-milling, 0.5 g of the powder sample was mixed with 15 mL of solvent and stirred at 70°C for 24 h using magnetic stirring with a rate of 120 rpm. The sample was then washed with 50 mL of distilled water, filtered, and dried under N_2 for 1 h at room temperature.

2.3. Characterization of Microstructure. XRD measurements were conducted on a Rigaku D/max-rA instrument using CuKα radiation with an accelerating voltage of 40 kV, a scanning range of 10°–90°, and a step size of 0.02° at the scan rate of 2.5° min^{-1}. The scanning electron microscope (SEM) was an Hitachi SU70 field emission SEM, and the transmission electron microscope (TEM) was a Fei Tecnai G2 F30 high resolution TEM. The specific surface area and pore size were analyzed using a specific surface area analyzer (Autosorb 1C, Quantachrome Co., Ltd.). The sample was degassed at 80°C for 24 h, and then the adsorption-desorption of N_2 at low temperature was tested to obtain the N_2 adsorption-desorption isothermal curve. The BET and BJH methods were used to calculate the specific area and pore size distribution of each sample.

2.4. Preparation of Coin Cell and Cycling Measurements. The obtained powder was dispersed in an appropriate amount of 1-methyl-2-pyrrolidone as a liquid slurry solvent and mixed well in a mortar. The slurry was then pasted onto Cu foil to form the electrode plates, and this was followed by a drying treatment in an oven at 60°C for 12 h and in vacuum oven at 120°C for 2 h. The electrode plates were placed in a glove box filled with high purity Ar. The prepared electrode plate was used as the working electrode, and pure lithium metal was used as the counter electrode. A Celgard 2325 diaphragm was used to separate the working electrode and counter electrode. Finally, electrolyte was infused, and a LIR2025 type coin cell was assembled in a sealing machine. The prepared coin cell was left to stand for 12 h, and then the charge-discharge measurements of the cells were carried out at room temperature using the Xinwei battery testing system at a current density of 175 mA g^{-1} or at higher rates within a voltage window of 0.01–3.00 V.

3. Results and Discussion

In contrast to previous work on the synthesis of lamellar Fe_3O_4 nanosheets prepared by one-pot solution method [23] and two-step microemulsion solvothermal approach [24], the strategy in this work is based on a purely mechanical synthesis. Especially, the Fe foil/flake graphite composite material is firstly in situ transited into lamellar Fe nanosheets/GNS composite after HPT treatment. The high energy influx by HPT further activated functional groups on the edges of flake graphite, made the flake graphite slip to the specific crystal orientation, and achieved the in situ generation of quasi-two-dimensional (2D) graphite nanosheets. We then used the specific chemical oxidation method to obtain Fe_3O_4 nanosheets and turned the original composite material system into the porous Fe_3O_4/GNS composites after short-time dispersion and drying. The approach introduced here is different from the conventional exfoliation approaches of 2D materials nanosheets in the activation process by using Li^+ insertion [25] and liquid stirring [26], and it is also different from the Hummers method for obtaining common graphene oxide [27].

3.1. Microstructure Characterization. Figure 2(a) shows the XRD pattern of the prepared sample, and it is consistent with the XRD patterns of the hydrothermal prepared Fe_3O_4/graphene nanosheets composite [28]. The diffraction peaks of Fe_3O_4 are in agreement with those of a face-centered cubic (FCC) structure of Fe_3O_4 (JCPDS no. 75-0033) and the expanded reflection peak of GNS indicates the low crystallinity and nanocrystal characteristics of HPT-processed sample.

SEM and TEM were used to characterize the surface morphology and microstructure of the dispersed Fe_3O_4/GNS material, as shown in Figure 2. In Figures 2(b)–2(d), it can be clearly seen that the sample contained a Fe_3O_4/GNS flower-like secondary structure due to no surfactant treatment. Each corresponding flower-like structure had the porous lamellar structure that was composed of many crinkled nanosheets connected to each other, as shown in Figure 2(b). TEM was used to further verify that the lamellar sheets are composite of Fe_3O_4 and GNS with large substrate sizes (Figure 2(c)). Interestingly, from the HRTEM image (Figure 2(d)), it can be verified that the interplanar spacing of $(2\ 2\ 0)$ was consistent with the XRD results shown in Figure 2(a). The large mechanical energy influx via HPT can uniformly expand the interplanar distance, and this is beneficial for forming the transmission path of Li^+. In addition, the porous Fe_3O_4/GNS structure is most likely to be an ideal Li storage material because of the potential of the high specific surface area and

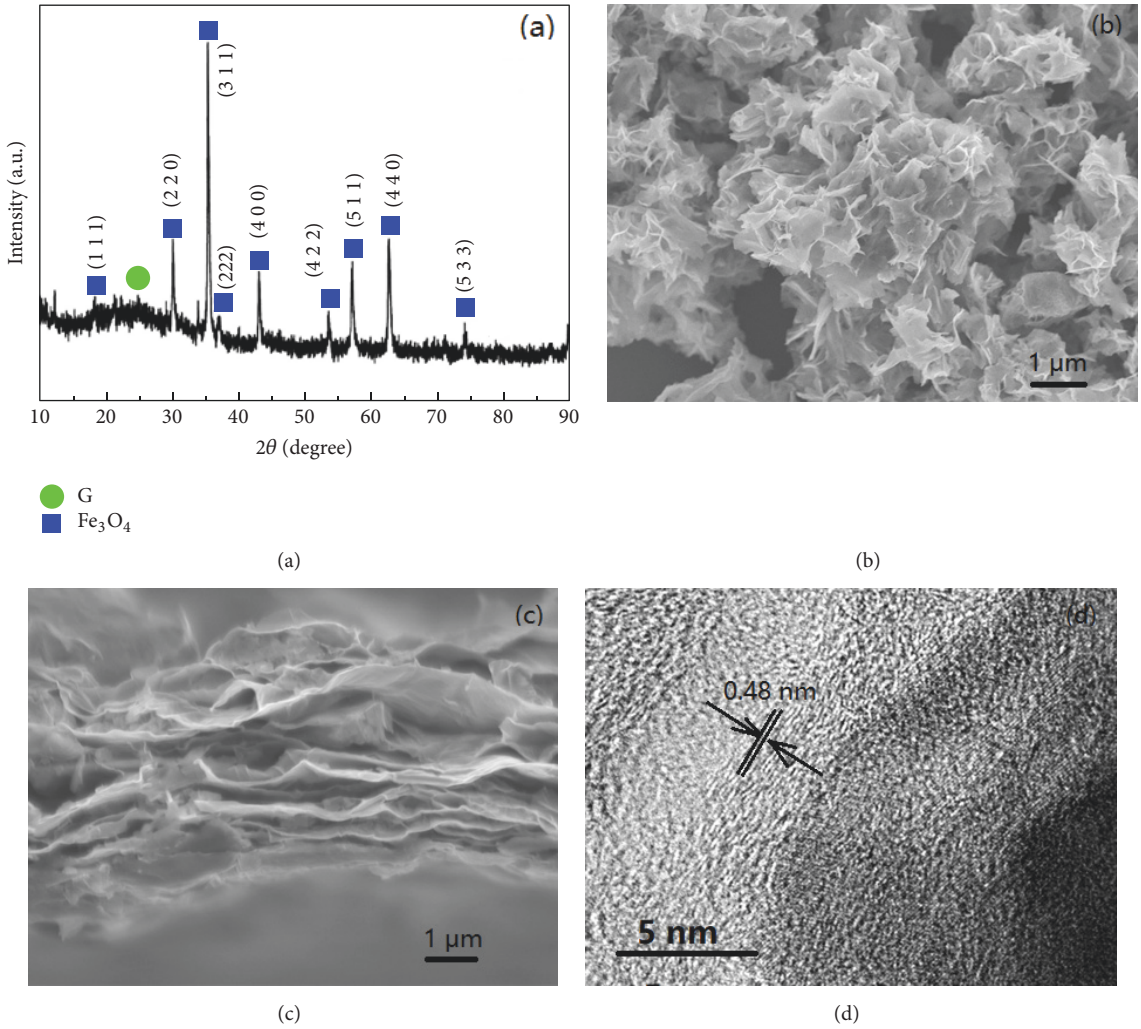

Figure 2: XRD pattern and microstructural characterization: (a) XRD pattern; (b) SEM image; (c) TEM image; (d) HRTEM image.

highly exposed 2D lamellar morphology to generate more Li^+ adsorption sites on the surface.

Next, N_2 adsorption/desorption experiments at 77 K were used to measure the specific surface area and pore structures. The curves in Figure 3 depict a typical type IV isothermal curve, indicating mesoporous characteristics. The Brunauer-Emmett-Teller (BET) specific surface area was determined to be 324 $m^2\,g^{-1}$ and the pore volume was 1.34 $cm^3\,g^{-1}$. The pore distribution diagram (the inset of Figure 3) exhibits the size distribution of mesopores. The distributions concentrated at around 80 nm and 200 nm, which verified the existence of the nanosize pores as proposed. This porous Fe_3O_4/GNS composite material can increase the electrode/electrolyte contacting interface and shorten the diffusion path of Li^+, thus relieving the volume change during Li^+ extraction and insertion process, and improve the lithium-storage simultaneously.

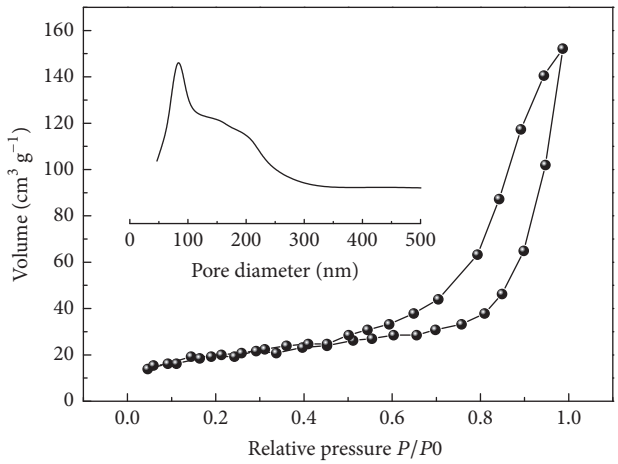

Figure 3: Specific surface area curves and pore distribution situation of as-achieved sample.

3.2. Electrochemical Properties. The electrochemical properties of the prepared Fe_3O_4/GNS composite were evaluated using a lithium half-cell. For comparison, the electrochemical performance of the composite prepared by high energy ball-milling method was also tested. Figure 4(a) shows the first three cycles of cyclic voltammetry (CV) curves of

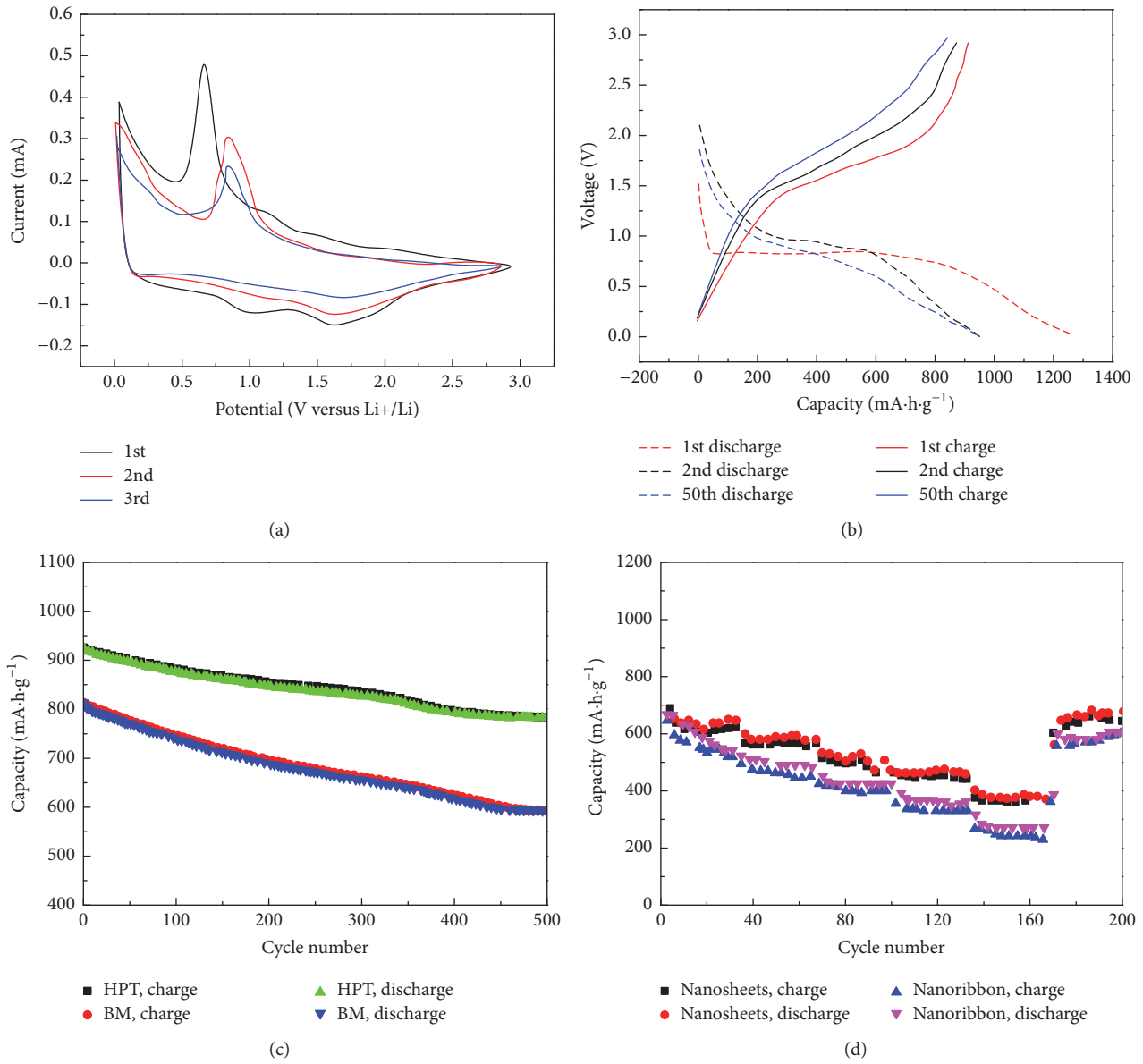

FIGURE 4: Electrochemical performance of as-prepared Fe_3O_4 composite materials: (a) CV curve of first three cycles tested at 0.1 mV s^{-1}, (b) first three discharge-charge curves at 1 C (350 mA h g^{-1}), (c) cycling performance at 1 C, and (d) rate capacity.

the Fe_3O_4/GNS composite sample. The voltage ranges from 0.01 V to 3 V at the scan rate of 0.1 mV s^{-1}. It can be clearly observed that the sharp oxidation-reduction peaks of the Fe_3O_4 phase mainly include a couple of sharp reduction peaks for Fe^{3+} to Fe^0 at 0.1 V and Fe^{2+} to Fe^0 at 0.6 V, as well as oxidation peaks for Fe^0 to Fe^{2+} at 1.6 V and Fe^{2+} to Fe^{3+} at 1.98 V. These findings indicate that there was an explicit ordering during the Li^+ insertion/extraction, and this can be related to the high energy influx from HPT within a short period of time. This energy input was transformed into a high density dislocation but did not drive surface amorphization of the Fe_3O_4 nanosheets. It can be seen from the corresponding capacitance performance that the graphite flakes in the samples are also partially exfoliated by HPT. The structure deflection and low crystallinity of GNS can provide a good inhibitor for volume expansion of crystalline Fe_3O_4 nanosheets. Then the corrugated ultrathin Fe_3O_4/GNS nanosheets composite formed the interpenetrating porous framework, which made the Li^+ and electron rapid transfer become possible. The large overlap of CV curves in the second and third cycles indicates improved reaction kinetics and the reversibility of the Fe_3O_4/GNS electrode. Figure 4(b) depicts the tilt charge/discharge curves of Fe_3O_4/GNS composite processed by HPT in the first three cycles. It can be seen from the first and second cycles that the HPT-processed Fe_3O_4/GNS composite electrode shows a high initial discharge capacity, charge capacities of 926 mA h·g^{-1} and 1241 mA h·g^{-1}, respectively, with a Coulombic efficiency of 75%. The initial irreversible capacity loss can be mainly ascribed to the decomposition of the trace water adsorbed

on electrode surface and to insertion of Li^+ ions to some unexfoliated sites. The Coulombic efficiency of the second discharging process rapidly increased to 96.5%, suggesting an excellent reversibility of the electrode. Figure 4(c) shows the cycling performance of both HPT-processed and high energy ball-milling processed electrode under 1 C (350 $mA \cdot g^{-1}$). Obviously, the HPT-processed electrode shows a higher storage capacity of Li^+ and high cycling stability. After 500 cycles, the reversible charge/discharge capacity remains at 783.1 $mA\,h \cdot g^{-1}$, and the retention rate is 88.8%, with respect to capacity value in the second cycle. In comparison, the high energy ball-milling processed electrode exhibits a similar capacity at 813.4 $mA\,h \cdot g^{-1}$ in the second cycle, the reversible capacity after 500 cycles drops significantly to 592.8 $mA\,h\,g^{-1}$, and the retention rate is only 72.9%. In addition, the HPT-processed electrode shows superior rate capacities of 881.5, 802.3, 712.4, 646.5, and 548.2 $mA\,h \cdot g^{-1}$ at rates of 0.5, 1, 2, 4, and 8 C, respectively. The reversible capacity remains at 798.7 $mA\,h \cdot g^{-1}$ as the rate is decreased back to 0.5 C, and this verifies the excellent rate capacity of the HPT-processed electrode. In comparison, for the high energy ball-milling processed electrode, the capacities at the rates of 0.5, 1, 2, 4, and 8 C are only 803.4, 702.8, 613.9, 572.4, and 505.3 $mA\,h \cdot g^{-1}$. The capacity remains at 764.3 $mA\,h\,g^{-1}$ as the cycling rate is decreased back to 0.5 C. The outstanding electrochemical performance of the HPT-processed Fe_3O_4/GNS composite nanosheet structure can be ascribed to the unique lamellar porous structure, ultrathin two-dimensional nanosheet morphology, and the entangled high density of dislocation (caused by HPT). Aforementioned factors greatly promoted the permeation of the electrolyte, largely decreased the Li^+/electron conduction path, and provided a large amount of surface sites for the rapid insertion/extraction of Li^+. Furthermore, comparing to hydrothermal and ball-milling synthesis, the highly dense bulk nanomaterial processed by the HPT is the electrode material with higher packing density, better electronic contacting, and shorter distance of ion transportation. Finally and importantly, the highly porous framework can effectively relieve the large volume change during insertion/extraction period, and the ultrahigh strength of the nanocrystal framework generated by HPT could also substantially improve the mechanical strength tolerance of the framework during the insertion/extraction period.

4. Conclusions

In this work, an efficient in situ preparation method for lamellar porous Fe_3O_4/GNS composite was introduced by using pure mechanical HPT processing method. The relevant electrochemical experiments confirmed that the obtained material has excellent high-rate capacity and cycling stability. The main advantages could be concluded as follows: the interconnected porous nanostructure and amorphous GNS provided high reversible capacity; high strength nanocrystalline framework generated by HPT confined volume expansion during Li^+ insertion period; the entangled high density dislocation created the rapid pathway for Li^+/electron diffusion.

Hereon, one of the most important concerns regarding using HPT to treat metallic materials is the HPT-induced physical phase transformation. In this case, specifically for iron-carbon system, we examine the carbide existence right after finishing the HPT treatment. From Fig. S1 in Supplementary Materials, with the low metal versus carbon material mass ratio, only trivial amount of Fe_3C has been found in the XRD pattern. The reason can be concluded in following: (1) grain refinement instead of second phase hardening is the main cold hardening mechanism during this process; (2) the generation of carbide needs at least 600–700°C annealing heat treatment and long time in iron-carbon system, but our process was under room temperature and completed in several minutes. Based on aforementioned evidence, the mechanical properties and phase transformation should be a factor to consider during raw material selection and experimental design stage. Even if the small amount of carbide is existing in the system, they will not affect the performance of alloy anode for lithium-ion batteries. On the other side, they can in fact contribute to capacity in some cases [29].

It is expected that the current SPD methods and equipment could be extended to manufacture many different functional metallic composite materials with application in energy storage and harvesting. However, as a top-down synthesis method for bulk nanomaterials, this approach is still restricted by some crucial important prerequisites, such as material plasticity and working hardening requirements, where further investigation and implementation is needed.

Conflicts of Interest

The authors declare that they have no conflicts of interest.

Authors' Contributions

Chenhao Qian and Ziyang He contributed equally.

Acknowledgments

This work was supported by the National Natural Science Foundation of China (11402264); the Natural Science Foundation of Jiangsu, China (BK20160182); and the Fundamental Research Funds from Jiangnan University, China (JUSRP116027, JUSRP51732B).

Supplementary Materials

Fig. S1: XRD pattern of HPT-processed sample without further chemical treatment. *(Supplementary Materials)*

References

[1] J. M. Tarascon and M. Armand, "Issues and challenges facing rechargeable lithium batteries," *Nature*, vol. 414, no. 6861, pp. 359–367, 2001.

[2] X. Zhu, Y. Zhu, S. Murali, M. D. Stoller, and R. S. Ruoff, "Nanostructured reduced graphene oxide/Fe_2O_3 composite as a high-performance anode material for lithium ion batteries," *ACS Nano*, vol. 5, no. 4, pp. 3333–3338, 2011.

[3] H. Buqa, D. Goers, M. Holzapfel, M. E. Spahr, and P. Novák, "High rate capability of graphite negative electrodes for lithium-ion batteries," *Journal of The Electrochemical Society*, vol. 152, no. 2, pp. A474–A481, 2005.

[4] A. S. Arico, P. Bruce, B. Scrosati, J.-M. Tarascon, and W. van Schalkwijk, "Nanostructured materials for advanced energy conversion and storage devices," *Nature Materials*, vol. 4, pp. 366–377, 2005.

[5] B. Jang, M. Park, O. B. Chae et al., "Direct synthesis of self-assembled ferrite/carbon hybrid nanosheets for high performance lithium-ion battery anodes," *Journal of the American Chemical Society*, vol. 134, no. 36, pp. 15010–15015, 2012.

[6] K.-A. Kwon, H.-S. Lim, Y.-K. Sun, and K.-D. Suh, "α-Fe2O3 submicron spheres with hollow and macroporous structures as high-performance anode materials for lithium ion batteries," *The Journal of Physical Chemistry C*, vol. 118, no. 6, pp. 2897–2907, 2014.

[7] B. Zhao, R. Liu, X. Cai et al., "Nanorod-like Fe2O3/graphene composite as a high-performance anode material for lithium ion batteries," *Journal of Applied Electrochemistry*, vol. 44, no. 1, pp. 53–60, 2014.

[8] J. Luo, J. Liu, Z. Zeng et al., "Three-dimensional graphene foam supported Fe3O4 lithium battery anodes with long cycle life and high rate capability," *Nano Letters*, vol. 13, no. 12, pp. 6136–6143, 2013.

[9] C. He, S. Wu, N. Zhao, C. Shi, E. Liu, and J. Li, "Carbon-encapsulated Fe_3O_4 nanoparticles as a high-rate lithium ion battery anode material," *ACS Nano*, vol. 7, no. 5, pp. 4459–4469, 2013.

[10] Y. Li, Q. Zhang, J. Zhu, X.-L. Wei, and P. K. Shen, "An extremely stable MnO2 anode incorporated with 3D porous graphene-like networks for lithium-ion batteries," *Journal of Materials Chemistry A*, vol. 2, no. 9, pp. 3163–3168, 2014.

[11] C. X. Guo, M. Wang, T. Chen, X. W. Lou, and C. M. Li, "A hierarchically nanostructured composite of MnO 2/conjugated polymer/graphene for high-performance lithium ion batteries," *Advanced Energy Materials*, vol. 1, no. 5, pp. 736–741, 2011.

[12] Z.-S. Wu, W. Ren, L. Wen et al., "Graphene anchored with Co_3O_4 nanoparticles as anode of lithium ion batteries with enhanced reversible capacity and cyclic performance," *ACS Nano*, vol. 4, no. 6, pp. 3187–3194, 2010.

[13] L. Tao, J. Zai, K. Wang et al., "Co 3O 4 nanorods/graphene nanosheets nanocomposites for lithium ion batteries with improved reversible capacity and cycle stability," *Journal of Power Sources*, vol. 202, pp. 230–235, 2012.

[14] Y. Wang, M. Xu, Z. Peng, and G. Zheng, "Direct growth of mesoporous Sn-doped TiO_2 thin films on conducting substrates for lithium-ion battery anodes," *Journal of Materials Chemistry A*, vol. 1, no. 42, pp. 13222–13226, 2013.

[15] Y. Ren, Z. Liu, F. Pourpoint, A. R. Armstrong, C. P. Grey, and P. G. Bruce, "Nanoparticulate TiO 2(B): An anode for lithium-ion batteries," *Angewandte Chemie International Edition*, vol. 51, no. 9, pp. 2164–2167, 2012.

[16] H. B. Wu, J. S. Chen, H. H. Hng, and X. W. D. Lou, "Nanostructured metal oxide-based materials as advanced anodes for lithium-ion batteries," *Nanoscale*, vol. 4, no. 8, pp. 2526–2542, 2012.

[17] M. V. Reddy, G. V. Subba Rao, and B. V. R. Chowdari, "Metal oxides and oxysalts as anode materials for Li ion batteries," *Chemical Reviews*, vol. 113, no. 7, pp. 5364–5457, 2013.

[18] L. Zhuo, Y. Wu, L. Wang et al., "CO2-expanded ethanol chemical synthesis of a Fe 3O4@graphene composite and its good electrochemical properties as anode material for Li-ion batteries," *Journal of Materials Chemistry A*, vol. 1, no. 12, pp. 3954–3960, 2013.

[19] P. Lian, X. Zhu, H. Xiang, Z. Li, W. Yang, and H. Wang, "Enhanced cycling performance of Fe_3O_4-graphene nanocomposite as an anode material for lithium-ion batteries," *Electrochimica Acta*, vol. 56, no. 2, pp. 834–840, 2010.

[20] R. Valiev, "Nanostructuring of metals by severe plastic deformation for advanced properties," *Nature Materials*, vol. 3, no. 8, pp. 511–516, 2004.

[21] Q. Wei, H. T. Zhang, B. E. Schuster et al., "Microstructure and mechanical properties of super-strong nanocrystalline tungsten processed by high-pressure torsion," *Acta Materialia*, vol. 54, no. 15, pp. 4079–4089, 2006.

[22] W. Zhao, M. Fang, F. Wu, H. Wu, L. Wang, and G. Chen, "Preparation of graphene by exfoliation of graphite using wet ball milling," *Journal of Materials Chemistry*, vol. 20, no. 28, pp. 5817–5819, 2010.

[23] G. Gao, S. Lu, B. Dong, Z. Zhang, Y. Zheng, and S. Ding, "One-pot synthesis of carbon coated Fe3O4 nanosheets with superior lithium storage capability," *Journal of Materials Chemistry A*, vol. 3, no. 8, pp. 4716–4721, 2015.

[24] C. Li, R. Wei, Y. Xu, A. Sun, and L. Wei, "Synthesis of hexagonal and triangular Fe3O4 nanosheets via seed-mediated solvothermal growth," *Nano Research*, vol. 7, no. 4, pp. 1–8, 2014.

[25] X. Rui, J. Zhu, W. Liu et al., "Facile preparation of hydrated vanadium pentoxide nanobelts based bulky paper as flexible binder-free cathodes for high-performance lithium ion batteries," *RSC Advances*, vol. 1, no. 1, pp. 117–122, 2011.

[26] K. R. Paton, E. Varrla, C. Backes et al., "Scalable production of large quantities of defect-free few-layer graphene by shear exfoliation in liquids," *Nature Materials*, vol. 13, no. 6, pp. 624–630, 2014.

[27] W. S. Hummers Jr. and R. E. Offeman, "Preparation of graphitic oxide," *Journal of the American Chemical Society*, vol. 80, no. 6, p. 1339, 1958.

[28] Y.-F. Mo, H.-T. Zhang, and Y.-N. Guo, "Fe_3O_4 nanoparticles dispersed graphene nanosheets for high performance lithium-ion battery anode," *Materials Letters*, vol. 205, pp. 118–121, 2017.

[29] M. Naguib, J. Come, B. Dyatkin et al., "MXene: a promising transition metal carbide anode for lithium-ion batteries," *Electrochemistry Communications*, vol. 16, no. 1, pp. 61–64, 2012.